Oncogene (2019) 38:3003–3018
https://doi.org/10.1038/s41388-018-0638-9

ARTICLE

Loss of ER retention motif of AGR2 can impact mTORC signaling and promote cancer metastasis

Katrin Tiemann[1] · Carolina Garri[1] · Sang Bok Lee[1] · Paymaneh D. Malihi[1] · Mincheol Park[1] · Ruth M. Alvarez[1] · Li Peng Yap[2] · Parag Mallick[3] · Jonathan E. Katz[1] · Mitchell E. Gross[1] · Kian Kani[1]

Received: 11 December 2017 / Revised: 29 October 2018 / Accepted: 21 November 2018 / Published online: 21 December 2018

Abstract

Anterior gradient 2 (AGR2) is a member of the protein disulfide isomerase (PDI) family, which plays a role in the regulation of protein homeostasis and the unfolded protein response pathway (UPR). AGR2 has also been characterized as a proto-oncogene and a potential cancer biomarker. Cellular localization of AGR2 is emerging as a key component for understanding the role of AGR2 as a proto-oncogene. Here, we provide evidence that extracellular AGR2 (eAGR2) promotes tumor metastasis in various in vivo models. To further characterize the role of the intracellular-resident versus extracellular protein, we performed a comprehensive protein-protein interaction screen. Based on these results, we identify AGR2 as an interacting partner of the mTORC2 pathway. Importantly, our data indicates that eAGR2 promotes increased phosphorylation of RICTOR (T1135), while intracellular AGR2 (iAGR2) antagonizes its levels and phosphorylation. Localization of AGR2 also has opposing effects on the Hippo pathway, spheroid formation, and response to chemotherapy in vitro. Collectively, our results identify disparate phenotypes predicated on AGR2 localization. Our findings also provide credence for screening of eAGR2 to guide therapeutic decisions.

Introduction

Anterior gradient 2 (AGR2) was initially isolated as a key gene in the development of the *Xenopus laevis* forebrain and its mucus-secreting cement gland [1]. In humans, AGR2 has an *N*-terminal endoplasmic reticulum (ER) leader sequence, a *C*-terminal ER retention sequence (KTEL) [2], and a catalytic cysteine (C81) homologous to the (C/SXXC/S) motif observed in members of the protein disulfide isomerase (PDI) family [3]. The role of AGR2 has thus been best characterized as a regulator of protein homeostasis and a member of the unfolded protein response pathway in the ER [4]. Extracellular AGR2 (eAGR2) is glycosylated [5] and known to interact with the extracellular matrix [6]. However, the molecular mechanism leading to secretion of AGR2 or its molecular function in the extracellular space has not been well defined.

AGR2 has also been described as a proto-oncogene and potential cancer biomarker. Wang et al. [7] first demonstrated that ectopic over-expression of AGR2 is sufficient for transformation of fibroblasts. In addition, a number of studies have linked AGR2 with cell invasion, migration, and the development of drug resistance in breast, lung, ovarian, prostate, and glioblastoma [8–15]. Several reports have utilized RNA or protein-based assays and determined that almost all adenocarcinomas display increased levels of AGR2 compared with adjacent normal tissue. Furthermore, increased AGR2 expression is correlated with cancer progression and metastatic disease in prostate, breast, pancreatic, and ovarian cancers [1, 16–21]. Nonetheless, expression of AGR2 is also correlated with positive clinical outcomes [9, 19, 22]. One possible explanation for the disparate prognostic correlation of AGR2 and patient

Supplementary information The online version of this article (https://doi.org/10.1038/s41388-018-0638-9) contains supplementary material, which is available to authorized users.

✉ Kian Kani
Kani@usc.edu

[1] University of Southern California, Keck School of Medicine, Lawrence J. Ellison Institute for Transformative Medicine, Los Angeles, CA, USA

[2] Department of Radiology, Keck School of Medicine, Los Angeles, CA, USA

[3] Stanford University, Department of Radiology, Los Angeles, CA, USA

outcomes may involve differences in AGR2 cellular localization.

Extracellular AGR2 has been shown to increase migration and invasiveness of cancer cells [6, 23, 24] and activate noncanonical Wnt signaling in colorectal cancer [25]. Yet, detailed studies that explicitly consider AGR2 cellular localization are lacking. Given the emerging role of AGR2 as a proto-oncogene and the lack of mechanistic insight on eAGR2 and tumor progression, we investigated the role of the iAGR2 versus eAGR2 in various in vivo, in vitro, and clinical specimens.

Results

Secreted AGR2 increases tumor mass and metastatic potential in xenograft mice

To investigate the significance of AGR2 cellular localization on tumor growth, we employed two metastatic cancer models. The first used a pancreatic cancer cell line (MiaPaCa-2) with no detectable AGR2. We performed non-invasive bioluminescent imaging to detect the tumor growth [26]. Single-cell clones of MiaPaCa-2 cells transduced with luciferase were subsequently used to create green fluorescent protein (GFP), wild-type (wt) AGR2, or AGR2 ΔKTEL sublines. We assessed the levels of iAGR2 and eAGR2 by immunoblot (Fig. 1A) and ELISA [27] (Supplementary Fig. 1). Expression of AGR2 ΔKTEL led to an increase in eAGR2 compared to the MiaPaCa-2 expressing wt AGR2. We injected 10 male athymic nude mice with 50,000 MiaPaCa-2 Luciferase GFP, AGR2 wt or AGR2 ΔKTEL per animal by intra-cardiac injection (Fig. 1B) and compared tumor burden by bioluminescent imaging. Three weeks post injection, the tumor size of mice with the AGR2 ΔKTEL constructs was significantly larger ($p < 0.05$) than the control or wt AGR2 tumor bearing mice (Fig. 1C) suggesting that the removal of the ER retention sequence promotes secretion of AGR2 and increases metastatic burden as compared to wt AGR2.

To further investigate the impact of eAGR2 on metastatic potential, we chose to treat prostate cancer xenograft mice with recombinant AGR2 (rAGR2) [28] (Supplementary Fig. 2), to achieve circulating levels comparable to that of men with castration-resistant metastatic prostate cancer [29]. We injected 50,000 CWR22-luciferase cells into the left ventricle of female athymic nude mice and subsequently either administered 100 ng of rAGR2/kg/week, or vehicle control intravenously (Fig. 1D). Tumor growth was assessed for up to 60 days with bioluminescence imaging (Fig. 1E). The percentage of mice with tumors was significantly higher upon dosing with rAGR2 ($p = 0.028$) (Fig. 1F), as was concomitant increase in tumor burden ($p < 0.05$) (Fig. 1G). Furthermore, mice treated with rAGR2 developed three metastatic lesions (lymph node, jaw, and leg) in contrast to none in vehicle treated mice (Fig. 1H-I). Taken together, our data suggests that increased concentration of eAGR2 has a distinct, metastasis-promoting role in vivo.

AGR2 interactome identifies proteins within Hippo and mTORC pathways

To elucidate the mechanism that either alters AGR2 cellular localization or identifies proteins and pathways that become differentially modulated when AGR2 is secreted, we employed a comprehensive protein–protein interaction study that maintains the spatial interactions in the whole-cell lysate and extracellular space. The combination of proximity-based biotinylation (BioID) [30] and targeted in vivo biotinylation of a biotin acceptor peptide epitope (BAP) provides two orthogonal methods to identify interacting proteins. We began by establishing PANC1, MiaPaCa-2 and MCF7 cell lines expressing BirA and AGR2_BAP or BAP_AGR2 as well as the N- and C-terminal BirA* AGR2 fusion protein (Supplementary Fig. 3). To ensure biotinlylation and similar expression pattern between endogenous AGR2 and overexpression of BioID constructs we performed gel electrophoresis and fluorescence microscopy (Supplementary Fig. 4). Cell lysates and spent media were subject to affinity purification followed by proteomic analysis of the intra- and extracellular AGR2 interactome (Fig. 2A). We used metabolic labeling of cells (I-DIRT [31]) in conjunction with elimination of common contaminant proteins (CRAPome [32]). We identified 66 (PANC1), 155 (MiaPaCa-2), and 365 (MCF7) AGR2-interacting proteins after applying stringent peptide and protein identification criteria (false discovery rate < 0.01) and removing contaminant proteins [28] (Fig. 2B).

We specifically wanted to incorporate a cell line with endogenous expression of AGR2 (MCF7) to ensure that pathways and proteins related to AGR2 are co-expressed. In fact, we enumerated more AGR2-interacting proteins in the MCF7 cell line than in PANC1 or MiaPaCa-2. In order to calibrate our results, we specifically examined each experiment for the positive identification of AGR2 and known interacting proteins (GRP78/HSPA5) [33] and (REPTIN and RUVBL2) [34, 35]. We identified AGR2 peptides in all experiments (Fig. 2C) and HSPA5 in all experiments derived from the whole-cell lysates (Table 1 and Table S1). Collectively, these results indicate that our interactome study was well-controlled.

We subsequently used the list of AGR2-interacting proteins and investigated their membership in various biological processes by ingenuity pathway analysis (Fig. 2D) (Table S2). The Hippo signaling was among the top 20

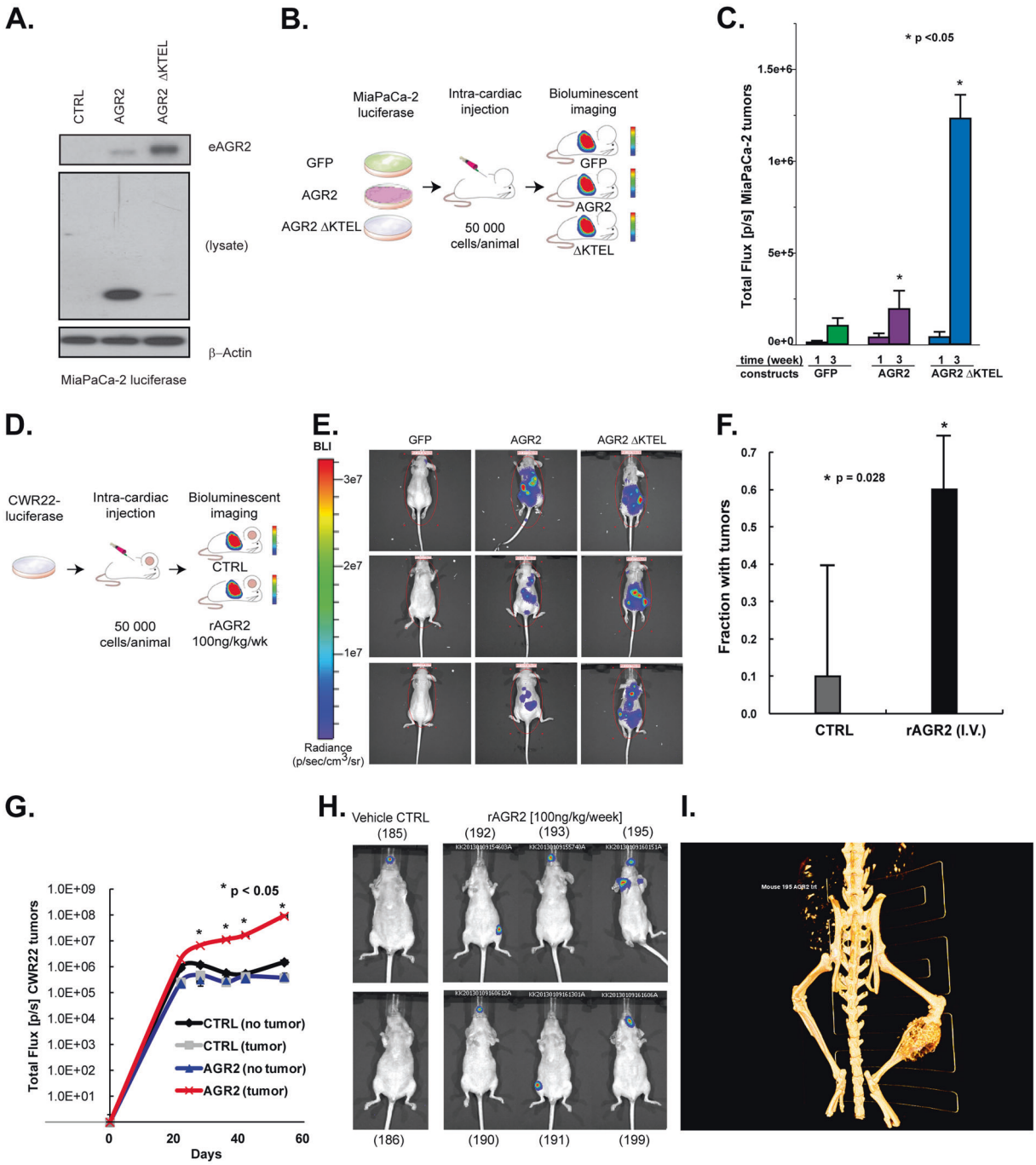

Fig. 1 eAGR2 promotes cancer metastasis in prostate and pancreatic cancer xenografts. **A** Loss of ER retention sequence (KTEL) increases levels of eAGR2 in spent media in MiaPaCa-2 cells. **B** MiaPaCa-2 pancreatic cancer cells carrying luciferase were transfected with GFP, AGR2 wt, and AGR2 ΔKTEL and were injected into left ventricle of ($N = 10$) nude mice (per arm) to investigate the impact of increased secretion of AGR2 and tumor growth. **C** Error bars are expressed as average ± SD. Results were normally distributed with equal variance between groups were analyzed by unpaired two-tailed Student's t test. Asterisks denote p value significance (Student's t test, $p < 0.05$) between AGR2 wt and AGR2 ΔKTEL. **D** Prostate cancer xenografts ($N = 10$ per arm) were injected with purified recombinant AGR2 by intravenous injection in the left ventricle show increased tumor incidence and **E**, **F** with higher flux **G**, **H** than control treated mice. Error bars are expressed as average ± SD. Results were normally distributed with equal variance between two groups and were analyzed by paired two-tailed Student's t test. Asterisks denote p value significance ($p < 0.05$). **i** Metastatic spread to right leg (red arrow) but not the left leg (gray arrow) was observed in two mice by CT scan (mouse #195)

pathways enriched in the AGR2 interactome across all experiments. The interactome screen also confirmed the interaction of eAGR2 with VEGF and other ligands known to promote angiogenesis [23]. We also noted that the

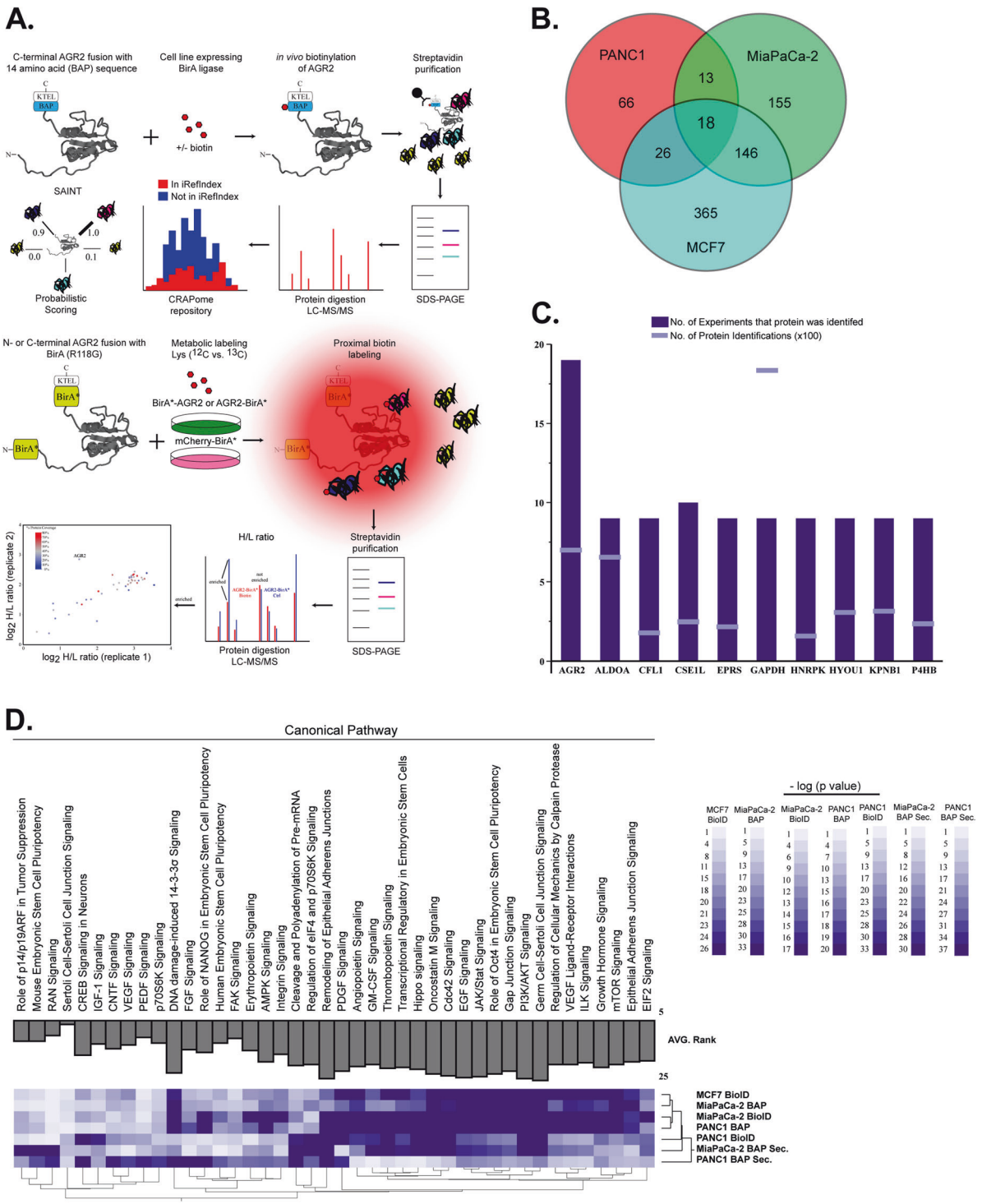

mTORC signaling pathway and its downstream effectors (EIF2, PI3K/AKT, ILK, and P70S6K) were highly enriched across all experiments. The only publication that implicates AGR2 and mTORC is in the context of 3′UTR shortening [36]. We set out to investigate the role of eAGR2 versus iAGR2 in the Hippo and mTORC pathways.

eAGR2 stabilizes phosphorylation of YAP1 independent of its PDI active site

The Hippo signaling pathway is involved in restraining cell proliferation and promoting apoptosis [37]. Increased Hippo pathway activity results in YAP1 phosphorylation, which

◀ **Fig. 2** Interrogation of AGR2-interacting partners in the ER and extracellular space. **A** We performed immunoprecipitation assays followed by mass spectrometry (MS) analysis of BAP-AGR2 and AGR2-BAP. Protein lists were submitted to CRAPome (contaminant repository for affinity purification) and SAINT (significance analysis of INTeractome) [54] analysis, which allowed the identification of high-scoring interactions. We also used proximity ligation of biotin to prey proteins by the expression of bait proteins fused to a nonspecific biotin ligase, BirA* (BioID). In vivo biotinylation of proximal proteins was detected by streptavidin-based affinity purification and proteomics identification. Isotopic labeling of cells with control (BirA* mCherry) transfected cells was used to refine proteins in the AGR2 interactome. **B** Total number of AGR2-interacting proteins after removal of contaminants. **C** AGR2 was identified in ($n = 19/19$) experiments derived from whole-cell lysates (although its expression levels were lower than high abundant contaminant proteins) (GAPDH). **D** New biological pathways ascribed to AGR2 were enriched by ingenuity pathway analysis. The AGR2 interactome was enriched for proteins that have been linked to the mTORC pathway in all three cancer cell lines used in this assay. We also noted that analysis of the AGR2 interactome in the extracellular (Secreted) space clustered differently that the whole-cell lysates (whole-cell lysates)

reduces transport from the cytoplasm to the nucleus (where it induces transcription as a co-activator with other DNA-binding proteins) leading to increased tumor growth. Increased levels of nuclear YAP1 favors cell proliferation, survival, and the acquisition of a cancer-promoting phenotype [38]. Since AGR2 expression has been shown to increase YAP1 nuclear localization [39] and the Hippo pathway was enriched in the whole-cell lysate and extracellular AGR2 interactome, we set out to discriminate the impact of AGR2 cellular localization on the induction of the Hippo pathway.

The prostate cancer cell line PC3 and breast cancer cell line MCF7 both express and secrete medium to high levels of AGR2 (Supplementary Fig. 1). We generated heterozygous PC3 and MCF7 AGR2 CRISPR/Cas9 knockouts cell lines and screened for total and phosphorylated YAP1. Both AGR2 knockout cell lines revealed an increase in p-YAP1 (Ser 127) without a concomitant increase in total YAP levels (Fig. 3A).

We subsequently employed DU145 and MiaPaCa-2 cells with undetectable AGR2 as platform to investigate whether differences in AGR2 localization would impact activation of the Hippo pathway. For this purpose, we generated DU145 and MiaPaCa-2 expressing GFP, AGR2, AGR2 ΔKTEL, and AGR2 C81S. AGR2 C81S was included to investigate whether the molecular changes in the identified pathways are dependent on the reported enzymatic active site (C81) of AGR2. We did not observe any appreciable change in total levels of YAP1 upon overexpression of any of the AGR2 constructs in the two cell lines (Fig. 3B). However, overexpression of AGR2 Δ KTEL and AGR2 C81S increased phosphorylation of YAP1 (Fig. 3b) in a manner which is commensurate with the levels of eAGR2 by ELISA (Supplementary Fig. 1), indicating that the enzymatic active site has a role in preventing YAP1 phosphorylation.

To exclude contribution from iAGR2 and further link YAP1 phosphorylation with the self-association state and PDI activity of eAGR2, we treated DU145 and MiaPaCa-2 cells over a course of 16 h with 100 nmol/l rAGR2 Δ27 (dimer), rAGR2 Δ27 C81S (dimer/PDI deficient), rAGR2 Δ27 E60Q (monomer), rAGR2 Δ41 (strongly dimeric), and BSA as control [2, 34]. The results indicate an increase in p-YAP1 (S127) with dosing of rAGR2, including the PDI deficient C81S. This suggests that eAGR2 is sufficient to promote phosphorylation of YAP1 irrespective of C81 (Fig. 3C). Moreover, a correlation with increased AGR2 self-association and levels of p-YAP1 (S127) was noted (Fig. 3C).

In order to confirm this finding and account for ER stress we treated MCF7 ΔAGR2 cells with each recombinant protein, BSA, dithiothreitol (DTT), and tunicamycin. Disruption of PDI activity by DTT or induction of ER stress by tunicamycin did not alter YAP1 expression or phosphorylation. Increased p-YAP1 was noted when the cells were treated with each recombinant protein (Fig. 3D).

Since transcriptional activity requires nuclear translocation of YAP1, we investigated the YAP1 distribution in the nuclear and cytosolic compartments of DU145 GFP, AGR2 wt, AGR2 ΔKTEL, and AGR2 C81S. Fractionation of cytosolic HSP90 and nuclear Lamin A/C provided a control for this experiment (Fig. 3E, F). DU145 transfected with GFP had the largest proportion of nuclear YAP1 (88%), while cells transfected with constructs that induced phosphorylation of YAP1 (ΔKTEL, C81S) had increased cytosolic YAP1 (62% and 53%, respectively) (Fig. 3E, F). Taken together, our results highlight a distinct role for phosphorylation and nuclear localization of YAP1 by eAGR2 that was independent of its PDI active site.

AGR2 alters mTORC2 signaling

The mTORC pathway integrates signaling cues from oncogenes and tumor suppressors via two distinct protein complexes (mTORC1 and mTORC2) [40]. Our interactome study identified RPS6 as a component of the AGR2 interactome thereby linking mTORC and AGR2 (Table S1). We verified this interaction by BioID in MCF7 and MiaPaCa-2 cells (Fig. 4A). Since RPS6 is one of the downstream readouts for RICTOR-T1135 phosphorylation [41, 42] we also performed co-immunoprecipitation (Co-IP) on components of the mTORC2 pathway. In MCF7 and PC3 cells, AGR2 interacts with RICTOR and P70S6K (Fig. 4B). IGF1 induced activation of mTORC2 did not alter interaction of

Table 1 Selected eAGR2 associating proteins identified by AP–MS/MS

GO	Protein	Description	SAINT	Protein ID's	GO	Protein	Description	SAINT	Protein ID's
Signaling receptor binding	MAGI2	Membrane associated guanylate kinase, WW and PDZ domain containing 2	1.00	40	Nucleic acid binding	ELAVL3	ELAV like RNA binding protein 3	1.00	21
	C3	Complement C3	1.00	22		MLL3	Lysine methyltransferase 2C	1.00	7
	AGR2	Anterior gradient 2, protein disulfide isomerase family member	1.00	21		PRKCSH	Protein kinase C substrate 80K-H	1.00	7
	DST	Dystonin	1.00	7		RNF20	Ring finger protein 20	1.00	5
	TLN1	Talin 1	1.00	7		SALL1	Spalt like transcription factor 1	1.00	5
	SDHAF1	Succinate dehydrogenase complex assembly factor 1	1.00	6		SCML2	Scm polycomb group protein like 2	1.00	5
	VWF	von Willebrand factor	1.00	5		ZNF512B	Zinc finger protein 512B	0.99	5
	CNOT1	CCR4-NOT transcription complex subunit 1	1.00	3		INSM2	INSM transcriptional repressor 2	1.00	4
	DOCK4	Dedicator of cytokinesis 4	1.00	3		MKI67	Marker of proliferation Ki-67	0.99	3
	TRIP12	Thyroid hormone receptor interactor 12	1.00	3		MLL	Lysine methyltransferase 2A	0.98	2
	LAMB2	Laminin subunit beta 2	0.98	2		NUCB1	Nucleobindin 1	0.97	2
	TACC2	Transforming acidic coiled-coil containing protein 2	0.98	2		ZNF285A	Zinc finger protein 285	0.98	2
Structural molecula	AKAP6	A-kinase anchoring protein 6	1.00	42	Prot. domain binding	HOXC4	Homeobox C4	1.00	8
	COL15A1	Collagen type XV alpha 1 chain	1.00	10		HOXC6	Homeobox C6	1.00	4
	C1orf68	Chromosome 1 open reading frame 68	1.00	5		SH3PXD2B	SH3 and PX domains 2B	1.00	4
	COL4A4	Collagen type IV alpha 4 chain	0.99	3		SRRM2	Serine/arginine repetitive matrix 2	0.98	2
	COL6A1	Collagen type VI alpha 1 chain	0.97	2	Intermediate filament	COL11A1	Collagen type XI alpha 1 chain	1.00	4
GTPase Binding	EXOC2	Exocyst complex component 2	1.00	8		COL5A3	Collagen type V alpha 3 chain	1.00	7
	DIAPH3	Diaphanous related formin 3	1.00	6		COL4A3	Collagen type IV alpha 3 chain	1.00	6
	RIMS4	Regulating synaptic membrane exocytosis 4	1.00	6		EPPK1	Epiplakin 1	1.00	6
Miscellaneous	ADH5	Alcohol dehydrogenase 5 (class III), chi polypeptide	1.00	9	Miscellaneous	NAA35	N(alpha)-acetyltransferase 35, NatC auxiliary subunit	1.00	6
	COL4A6	Collagen type IV alpha 6 chain	1.00	9		KIAA1486	Neuronal tyrosine-phosphorylated phosphoinositide-3-kinase adapter 2	0.97	2
	TRPM1	Transient receptor potential cation channel subfamily M member 1	1.00	7		CSMD2	CUB and Sushi multiple domains 2	1.00	6
	DCHS1	Dachsous cadherin-related 1	0.98	2		FAM179B	TOG array regulator of axonemal microtubules 1	1.00	11
	AKAP13	A-kinase anchoring protein 13	1.00	165		SPATA7	Spermatogenesis associated 7	1.00	9
	FLJ43859	SPATA31 subfamily D member 4	1.00	15		MTUS2		1.00	5

Table 1 (continued)

GO	Protein	Description	SAINT	Protein ID's	GO	Protein	Description	SAINT	Protein ID's
							Microtubule associated scaffold protein 2		
	EHBP1	EH domain binding protein 1	1.00	4		COPS3	COP9 signalosome subunit 3	1.00	4
	KIAA1529	Coiled-coil domain containing 180	1.00	7		CSPP1	Centrosome and spindle pole associated protein 1	1.00	7
	CEP110	Centriolin	1.00	6		RNF123	Ring finger protein 123	0.98	2
	FSD1L	Fibronectin type III and SPRY domain containing 1 like	1.00	40		TPSG1	Tryptase gamma 1	1.00	12
	SPACA3	Sperm acrosome associated 3	0.99	3		AKAP6	A-kinase anchoring protein 6	1.00	42
	TET1	Tet methylcytosine dioxygenase 1	1.00	3		FLJ31713	Unkown	1.00	11
	LCK	LCK proto-oncogene, Src family tyrosine kinase	0.99	3		LOC441722	Unkown	0.99	3

For each interacting protein, the number of protein counts (FDR < 0.05) and corresponding SAINT score is given. Gene ontology molecular function is listed

AGR2 with the mTORC2 complex, suggesting that the interactome is independent of P70S6K kinase activity. We additionally confirmed that AGR2 binds RICTOR irrespective of its phosphorylation status by performing Co-IP in HEK293 cells expressing HA-RICTOR/T1135A/T1135D (Fig. 4C). We did not observe interaction between AGR2 and RAPTOR (mTORC1) (Supplementary Fig. 5).

These results indicate that AGR2 interacts with several components of the mTORC2 complex and may alter its signal transduction. We subsequently compared the ligand induced phosphorylation of several mTORC2 components in PC3 and PC3 ΔAGR2 cells. Treatment of PC3 cells with EGF, IGF, and insulin-triggered phosphorylation of RICTOR and AKT without robust phosphorylation of RPS6 (Fig. 4D). Knockout of AGR2 partially restored induction of RPS6 phosphorylation in PC3 cells (Fig. 4D). We noted an increase in basal phosphorylation of RICTOR (T1135) in PC3/PC3 ΔAGR2 and MCF7/MCF7ΔAGR2 cells (Fig. 4E) without induction of RPS6 phosphorylation. In order to confirm the association between AGR2 localization and RICTOR-1135 phosphorylation we utilized models without endogenous AGR2. We treated MiaPaCa-2 and DU145 cells with 100 nmol/l of rAGR2. Recombinant AGR2 increased phosphorylation of RICTOR (T1135) (Fig. 4F). Dosing of these two cell lines with rAGR2 C81S also increased phosphorylation of RICTOR (T1135), suggesting that the PDI active site is dispensable once AGR2 is secreted. The addition of an AGR2-neutralizing antibody inhibited phosphorylation of RICTOR (T1135) compared to untreated or isotype control antibody in cells with high endogenous levels of eAGR2 in MCF7 (Fig. 4G and Supplementary Fig. 1).

Overexpression of AGR2 in human bronchial epithelial cells, as well as addition of rAGR2 to AGR2 knock-down cell lines, has been shown to facilitate organoid formation [6]. Since eAGR2 promotes phosphorylation of RICTOR, we hypothesized that inhibitors targeting the mTOR pathway would have a dramatic effect on cancer cell spheroid formation, especially when dosed with rAGR2. Overexpression of wt AGR2 in MiaPaCa-2 cells reduced the spheroid formation potential compared to GFP control, but the AGR2 Δ KTEL cells were able to form spheroids within 48 h (Fig. 4H). Addition of 100 nmol/l rAGR2 to AGR2 wt MiaPaCa-2 cells enhanced spheroid formation. Upon treatment with dual mTORC1/2 inhibitor (OSI, 1 μmol/l) the capacity of MiaPaCa-2 cells to form spheroid was abolished. Once again, this phenotype was partially rescued by addition of rAGR2 (Fig. 4H).

To reveal the correlation between AGR2 and RICTOR in vivo, we performed integrative analysis of genomic data sets from The Cancer Genome Atlas (TCGA) [43, 44]. We first identified data sets with reverse phase protein array readouts on mTORC pathway and compared them to the

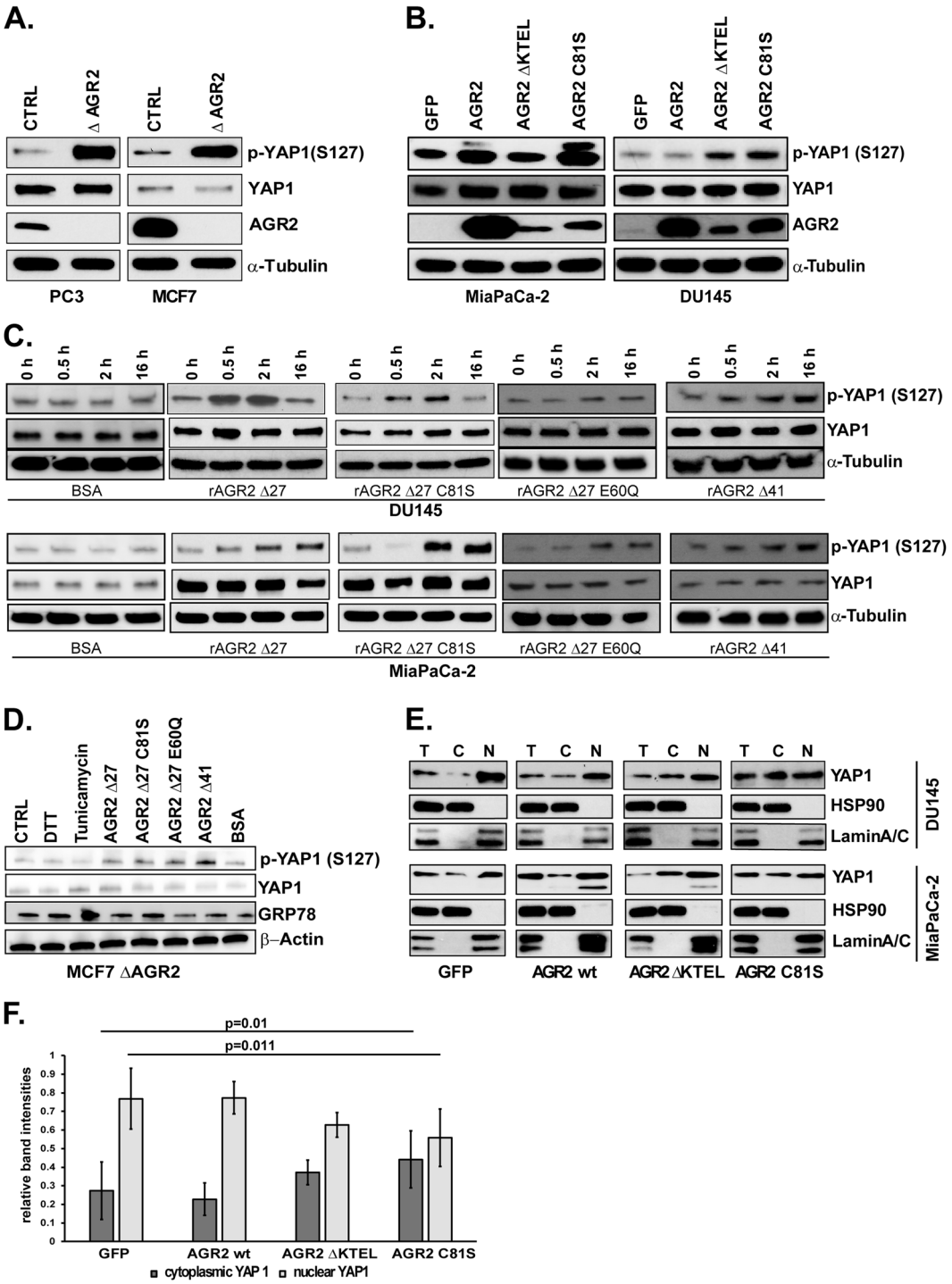

Fig. 3 eAGR2 alters activation of Hippo pathway via phosphorylation of YAP1. **A** Knockout of AGR2 in PC3 and MCF7 cell lines. Lysates were analyzed by immunoblot. **B** Overexpression of GFP, AGR2 wt, AGR2 ΔKTEL, and AGR2 C81S in MiaPaCa-2 and DU145 cells Lysates were analyzed by immunoblot. **C** Treatment of DU145 and MiaPaCa-2 cell lines with 100 nmol/l rAGR2 Δ27, rAGR2 Δ27 C81S, rAGR2 Δ27 E60Q, and rAGR2 Δ41 over 0.5, 2, and 16 h. Totally, 100 nmol/l of BSA was used as control. **D** MCF7 ΔAGR2 cells were treated with 1 mM DTT, 100 nmol/l BSA, 100 nmol/l rAGR2 or 5 µmol/l Tunicamycin for 2 h. Untreated cells were used as control (CTRL). Expression of UPR marker GRP78, p-YAP1, YAP1, and β-Actin were determined by western blot. **E** Nuclear and cytosolic fractionation of DU145 and MiaPaCa-2 lysates transfected with GFP and wt AGR2, AGR2 Δ KTEL, or AGR2 C81S were analyzed by immunoblot. **F** Quantitation of the immunoblots of five independent fractionation experiments (ImageJ) of DU145 cells. A two-tailed Student's *t* test was used to assess statistical significance ($p = 0.01$ and $p = 0.011$). All immunoblots are representative of data from at least three independent biological replicates

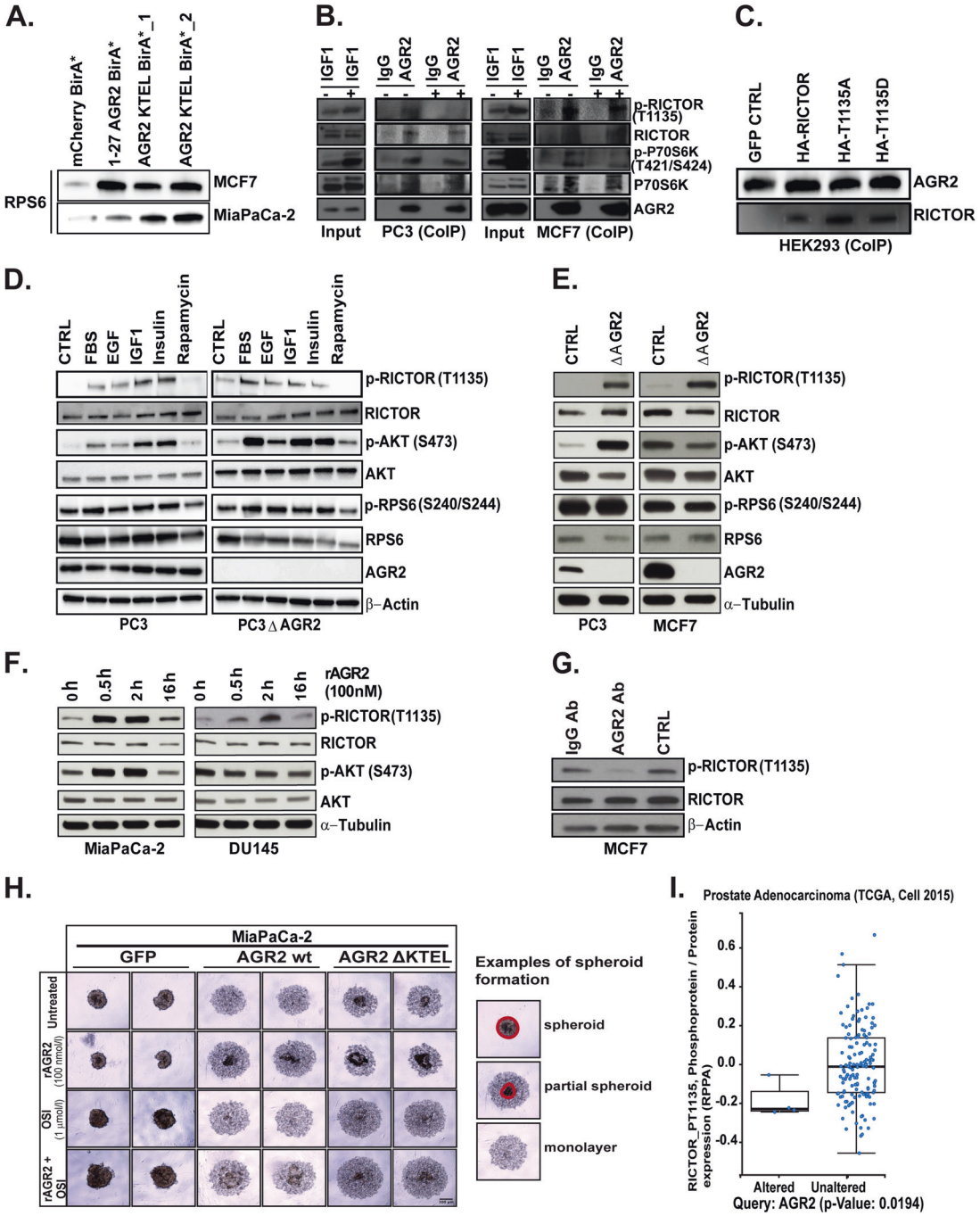

median expression of AGR2. In the provisional prostate [44] cancer data sets, we observed a significant correlation between pRICTOR (T1135) and AGR2 in patients with altered AGR2 expression (Fig. 5A). Moreover, co-expression of the top 20 genes with AGR2 showed enrichment of pRICTOR and YAP1 (Supplementary Fig. 6). Taken together, these findings indicate that cellular localization of AGR2 differentially alters mTORC2 signaling.

Juxtacrine AGR2 promotes tumor growth

We sought to investigate the impact of juxtacrine eAGR2 on tumor growth by utilizing the DU145 cell line transfected with AGR2 wt, ΔKTEL, or C81S which account for cellular localization and PDI activity of eAGR2 (Supplementary Figs. 1 and 6). Assessment of AGR2-naïve neighboring tumors will provide a suitable readout for juxtacrine signaling through eAGR2. We injected 1×10^6

◀ **Fig. 4** AGR2 interacts with mTORC2 complex thereby altering its signaling and cellular phenotype. **A** Stably transfected MCF7 and MiaPaCa-2 cells with AGR2 BioID constructs were subject to streptavidin pulldown and subsequently analyzed by immunoblot for RPS6 interaction with AGR2. As control mCherry BirA* was used. **B** Co-Immunoprecipitation (CoIP) of endogenous AGR2 or isotype matched IgG in PC3 and MCF7 cells under serum starvation (CTRL) or treated with 50 nmole/l IGF1 for 2 h. Cell lysates corresponding to input and CoIP fractions were subject to immunoblot for RICTOR/p-RICTOR, p-P79S6K/P70S6K with AGR2. **C** CoIP of transient transfected HEK293 cells with HA-RICTOR, HA-RICTOR-1135A, and HA-RICTOR-1135D cDNA. Cell lysates were incubated with biotinylated AGR2 (6 h) and precipitated with streptavidin magnetic beads. Immunoblot of the elute was probed for AGR2 and RICTOR. **D** PC3 and PC3 ΔAGR2 cell lines were serum starved or treated with 10% FBS, EGF (25 ng/ml), IGF1 (40 ng/ml), Insulin (250 nmol/l), and Rapamycin (20 nmol/l) for 2 h. The lysates were subjected to immunoblot for RICTOR, AKT, and RPS6. **E** Whole-cell lysates corresponding to knockout of AGR2 in PC3 and MCF7 cells were subject to immunoblot for mTORC2 (RICTOR) and its downstream components. **F** Time-course of MiaPaCa-2 and DU145 cells treated with rAGR2 and probed for RICTOR and AKT. **G** Treatment of MCF7 cells with AGR2 neutralizing antibody (500 nmole/l) or IgG (500 nmole/l) for 24 h. Lysates were subject to immunoblot of RICTOR. **H** Spheroid formation assay of pancreatic cancer cell lines transfected cells with GFP, AGR2 wt, and AGR2 DKTEL while treated with (PBS/untreated), rAGR2 with and without OSI 1 µmole/l for 48 h postplating. Spheriod formation was imaged by microscopy. An example of spheroid initiation formation is indicated by the drawn circles around the denser spheroid area. Area outside are cells not participating yet. **I** Correlation of AGR2 expression and phosphorylation of RICTOR in independent cohorts of patients with pancreatic (TCGA) and prostate adenocarcinomas [44] (unpaired Student's *t* test). All in vitro experiments represent at least three independent biological replicates

DU145 GFP subcutaneous into the flanks of female mice (randomized left or right flank). The contralateral flank was injected with either AGR2 wt, Δ KTEL or C81S expressing DU145 cells (Fig. 5B). We measured both tumor sites per mice up to day 18; upon which mice were sacrificed due to tumor burden. While the volume of AGR2 wt, AGR2 ΔKTEL, and AGR2 C81S tumors did not differ significantly, the contralateral GFP tumors opposite of the AGR2 ΔKTEL tumors were significantly larger ($p < 0.05$) (Fig. 5C). DU145 GFP tumors contralateral to AGR2 wt tumors were smaller than AGR2 C81S ($p < 0.05$) (Fig. 5D). These findings suggest that eAGR2 has the capacity to influence tumor growth at distant sites in our tumor models.

Response to docetaxel is predicated on cellular localization of AGR2

AGR2 has been shown to contribute to cytotoxic drug resistance to various DNA damaging agents both in vitro and in mouse xenografts [45]. However, the distinction between iAGR2 versus eAGR2 on response to chemotherapy has not been investigated. We examined the relationship between AGR2 expression and response to chemotherapy in prostate cancer. Men treated with chemotherapy have a significantly improved prognosis when AGR2 is overexpressed ($p = 0.0069$) (Fig. 6A). Moreover, we examined the expression of AGR2 in circulating tumor cells (CTC) obtained from men with metastatic prostate cancer treated with docetaxel. Our data indicates that patients that are sensitive to docetaxel have increased AGR2 expression in CTCs (lower ΔCt, Fig. 6B). In both of these independent clinical data sets, elevated levels of AGR2 predict a favorable response.

Clinical data sets with matching mRNA expression and serological levels of AGR2 from patients treated with chemotherapy are lacking. Therefore, we utilized in vitro models to assess the impact of AGR2 localization on response to docetaxel. DU145 cells were transfected with GFP, AGR2 wt, AGR2 C81S, and AGR2 ΔKTEL (Supplementary Figs. 1 and 7). We selected stable cell lines carrying each transgene and subjected them to cell viability assays. Overexpression of AGR2 wt sensitized cells to docetaxel, while AGR2 C81S did not impact IC50 (Fig. 6C). Cells transfected with AGR2 ΔKTEL, however, demonstrated significant resistance to docetaxel ($p < 0.05$). To confirm the docetaxel resistance promoting phenotype of eAGR2, we pretreated each cell line with 100 nmol/l of rAGR2 for 48 h prior to treatment with docetaxel. Our data indicate that rAGR2 is sufficient to increase docetaxel IC50, confirming the duality in response as a function of AGR2 localization ($p < 0.05$) (Fig. 6C).

Discussion

We set out to resolve disparate clinical outcome data ascribed to AGR2. We hypothesized that eAGR2 may promote cancer growth while iAGR2 might antagonize it; thereby implying that AGR2 cell localization is a key regulatory element. In our data, eAGR2 enhanced the metastatic potential of pancreatic cancer cells to peripheral organs and prostate cancer cells to the skeletal system (Fig. 1). Juxtacrine signaling of eAGR2 promotes increased growth of subcutaneous xenograft prostate cancer cells (Fig. 5). These finding are in accordance with reports of poor prognosis of patients with elevated eAGR2 in various body fluids [18, 29, 46, 47]. However, the exact molecular mechanism that differentiates eAGR2 versus iAGR2 is unknown.

In order to gain a better understanding of the role of eAGR2 and iAGR2 we utilized a combination of proximity ligation by BioID [48] and AP–MS/MS with cDNA constructs that preferentially secrete or maintain AGR2 intracellular. We initially focused on the Hippo and mTORC pathway as means to study the role of eAGR2 versus iAGR2. Our data suggest that AGR2 interacts with core

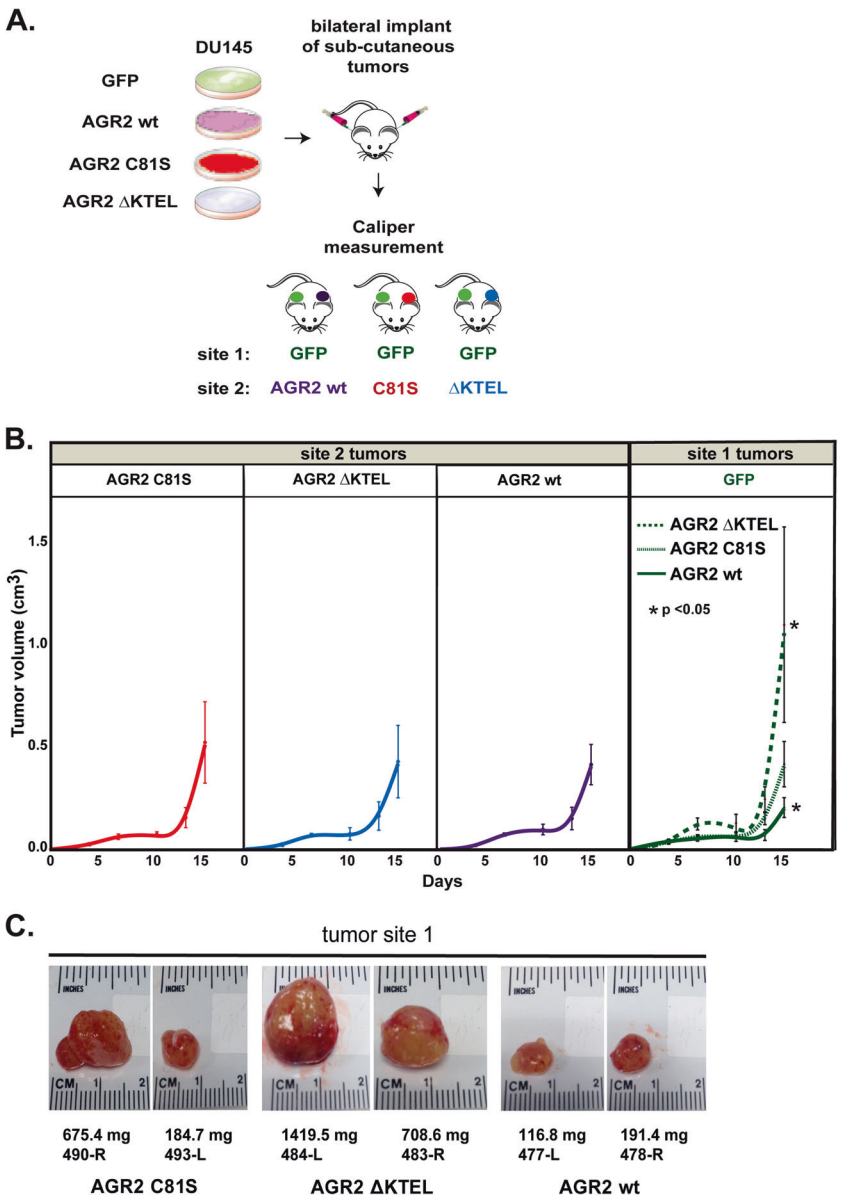

Fig. 5 Loss of ER retention motif promotes contralateral tumor growth. **A** Prostate cancer xenografts were used to assess the impact of juxtacrine AGR2 on contralateral tumor growth ($n = 8$). **B** DU145 mouse tumors at site 1 contralateral to AGR2 ΔKTEL are significantly larger ($p < 0.05$) than wildtype tumors contralateral to AGR2 or AGR2 C81S (Student's t test, $n = 8$). Site 2 tumors show no significant differences in size. **C** Two dissected tumors of site 1 (GFP tumor) collateral to AGR2 ΔKTEL, AGR2 C81S, and AGR2 wt. The tumor location, mouse number, and weight of tumor are displayed

components of the mTORC2 complex (RICTOR, RPS6, and P70S6K) (Fig. 4A) and eAGR2 promotes phosphorylation of RICTOR, whereas iAGR2 is antagonistic (Fig. 4D, E). We also noted that the PDI activity of eAGR2 is not required for induction of RICTOR or Hippo pathways (Figs. 3 and 4), indicating that there must be two distinct protein interfaces that govern AGR2 activity. Importantly, our findings indicate that the expression levels of AGR2 and factors that govern its secretion must be studied in context in order to understand either Hippo or mTORC2 signaling.

There are a number of outstanding questions regarding eAGR2 in cancer. The first set of questions pertains to the clinical utility of eAGR2 as a biomarker. For example, should cancer patients with elevated levels of serological eAGR2 be given mTORC inhibitors? Our data suggest that AGR2 interacts with various components of the mTORC2 complex thereby remodeling its downstream signaling. In addition, spheroid formation was attenuated by treatment with mTORC inhibitors in the presence of eAGR2 (Fig. 4I); further confirming this rationale. Moreover, the significance of AGR2 expression in patient CTCs is still unknown. In our limited patient cohorts, expression of AGR2 mRNA in CTCs seems to indicate favorable response to chemotherapy while increased serological eAGR2 predicts poor response (Fig. 6). Breast cancer patients with increased AGR2 mRNA in CTC clusters also had poor prognosis [49], confirming that increased AGR2 in CTCs is negatively associated with survival. Second, what is the role of eAGR2 on the tumor microenvironment? In our murine cancer model, eAGR2 was sufficient to remodel the metastatic niche in the murine skeletal system leading to osteolytic bone destruction (Fig. 1I).

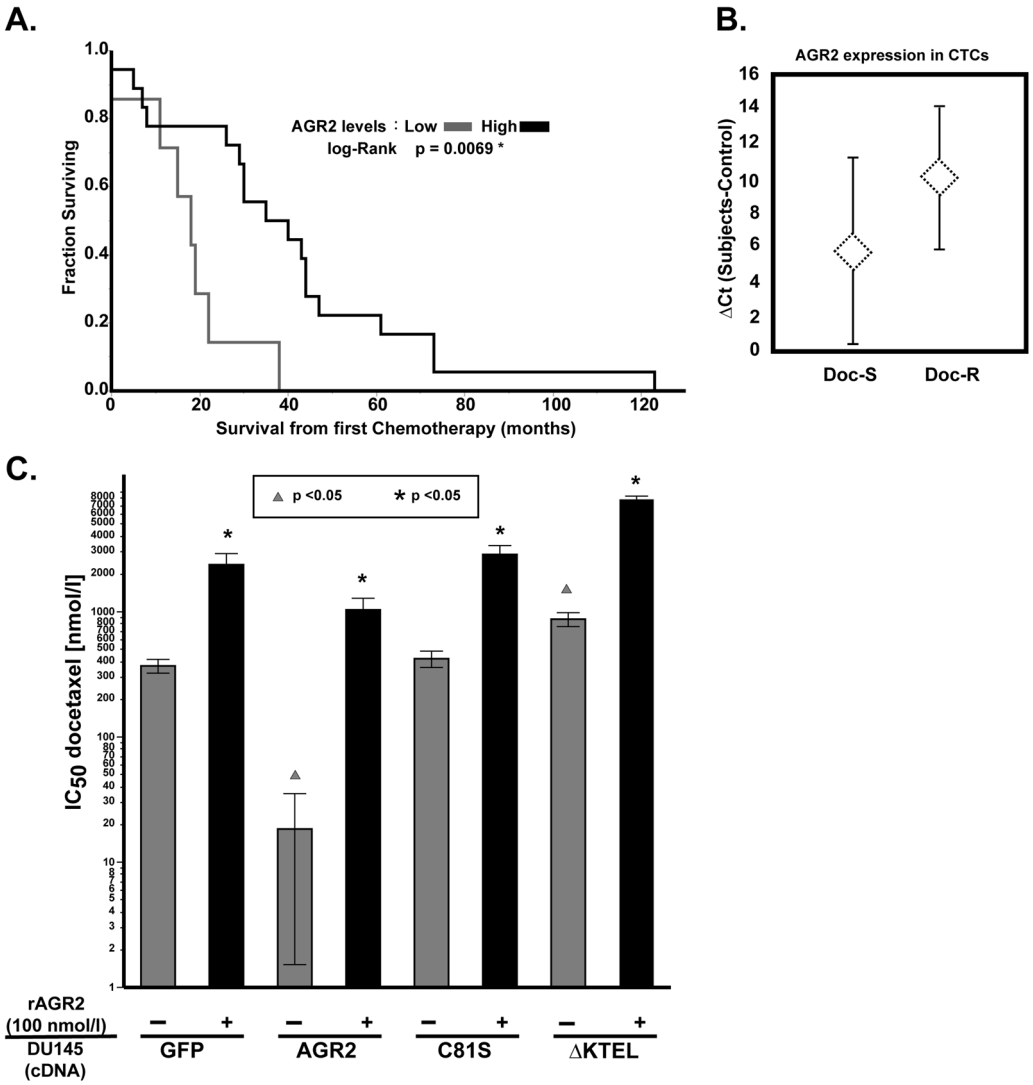

Fig. 6 Clinical significance of AGR2 expression in prostate cancer patients treated with chemotherapy. **A** Prostate cancer patients with high-AGR2 mRNA levels (median) have significantly longer survival from first chemotherapy (Mann–Whitney–Wilcoxon test, $p = 0.0069$). **B** AGR2 expression is increased in CTC-enriched peripheral blood (7.5 ml) obtained from CRPC patients prior to initiating docetaxel treatment the mean AGR2 expression (±SD) from CTC-enriched RNA in docetaxel-sensitive (Doc-S, $n = 15$) and docetaxel-resistant (Doc-R, $n = 7$) subjects were examined by RT-PCR. Docetaxel response is defined as a ≥30% reduction in PSA at 12 weeks as suggested by PSAWG2 guidelines [55]. We observe a strong trend towards increased AGR2 expression in the Doc-R cohort, which approaches statistical significance (Student's t test, $p = 0.06$). **C** DU145 parental or DU145 transfected with GFP, ΔKTEL, or C81S were treated with docetaxel for 48 h and treated with rAGR2 (100 nmol/l). Cell viability was assessed by MTS assay and IC50 was determined. Comparison of dosing with rAGR2 (100 nmol/l) is statistically represented by asterisks (Student's t test, $p < 0.05$). Comparison of transfection with AGR2 cDNA constructs (GFP as the reference) is statistically represented by triangles (Student's t test, $p < 0.05$). All experiments represent at least three independent biological replicates

Since AGR2 is not expressed in bone marrow [50], it is likely that eAGR2 may be acting on resident pathways to remodel the microenvironment. Other pathways known to remodel the microenvironment were also identified in our interactome data (angiogenesis and integrin signaling). Finally, little is known about the structural features governing AGR2's PDI activity and self-association. In our data, rAGR2, irrespective of its PDI active site, was able to increase phosphorylation of YAP1 (Fig. 3). We also noted a trend toward increased YAP1 phosphorylation with mutations in rAGR2 that enhanced dimerization (Δ41) compared to monomeric AGR2 (E60Q) in MiaPaCa-2 and DU145 cells (Fig. 3E). This trend was also evident when comparing the binding of AGR2 with REPTIN [34]. Interestingly, the interaction between eAGR2 and VEGF seems to involve both its PDI active site (C81) [51] and self-association state [23]. Preclinical development of small molecules or biologics targeting AGR2 must consider its expression in the tumor and adjacent microenvironment, juxtacrine signaling, PDI activity, and oligomerization.

Materials and methods

Cell lines

We purchased MCF7, PC3, DU145, MiaPaCa-2, HEK293, and PANC1 cells from ATCC and Lenti-X 293T cells from Clontech and used within 6 months of thawing. Cells were grown in DMEM (Fisher Scientific) media supplemented with 10% fetal bovine serum (Gemcell) or SILAC DMEM (SILAC Protein Quantitation kit-DMEM, Thermo Scientific) contained dialyzed FBS (Thermo Scientific) and either heavy or light Lysine (Thermo Scientific). Cells were grown at 37 °C with 5% CO_2.

Construct and stable cell line generation

The DNA constructs AGR2 BAP KTEL, AGR2 BAP ΔKTEL, 1–27 AGR2 BirA and AGR2 BirA KTEL were synthesized by Genewiz. The genes were PCR amplified and cloned into pLVX-IRES-Neo Vector (Clontech). The CMV BirA mCherry (pBY2982) was a gift from Ralf Baumeister (Addgene plasmid # 23220) and cloned into pLVX-IRES Puro (Clontech). The BirA R118G mutation (BirA*) was achieved with Agilent Technologies Quick Change II Site-Directed Mutagenesis kit following the manufacturer's instruction. Constructs were confirmed by sequencing (Genewiz). pCMV-VSV-G was a gift from Bob Weinberg (Addgene plasmid #8454). psPAX2 was a gift from Didier Trono (Addgene plasmid # 12260).

Stable cell lines were made with lentiviral particles as previously described [28]. Recombinant AGR2 was produced and validated as previously described [27].

AGR2 interactome

After six doublings in SILAC media stable cell lines (AGR2 BAP KTEL and AGR2 BAP ΔKTEL) were incubated for 24 h with or without 50 µM biotin. The cells were lysed as previously described [28]. One micro gram of unbiotinylated light-treated lysate was mixed with 1 mg biotinylated SILAC heavy lysate and vice verse. Spent media and lysates were incubated overnight with 150 µl Pierce™ Streptavidin Magnetic Beads (Thermo Scientific) and processed for MS as previously described [28].

Western blot analysis

Biotinylation, AGR2 IP and AGR2 BioID elution were verified by Western blot analysis with IRDye® 800 CW Streptavidin antibody (Licor) 1:1000 dilution in Odysee® blocking buffer (Licor). Normal mouse IgG CNTRL antibody for IP (Cat# sc-2342), AGR2 antibody (6C5) (Cat# sc-101211), were purchased from Santa Cruz. Phospho-YAP (Ser127) (D9W21) (Cat#13008), YAP (D8H1X) XP® Rabbit mAb (Cat#14074), Phospho-RPS6 rabbit (Ser240/244) (Cat#2215), RPS6 (5G10) rabbit mAB (Cat#2217), RPS6 (54D2) mouse mAb (Cat#2317), p70 S6 kinase (49D7) rabbit mAB (Cat#2708), phosphor-p70 S6 kinase (Thr389) (108D2) rabbit mAB (Cat#9234), Rictor (53A2) Rabbit mAb (Cat#2114), phospho-Rictor (Thr1135) (D30A3) rabbit mAb (Cat#3806), Akt (pan) (40D4) mouse mAb (Cat#2920), phosphor-Akt (Ser473) (D9E) rabbit mAb (Cat#4060) were purchased from Cell Signaling Technologies. Alpha-Tubulin (DM1A) mouse mAb (Cat#T9026) and beta-Actin (AC-15) mouse mAb (Cat#A1978) were purchased from Sigma-Aldrich. Anti-HA antibody was purchased from Thermo (26183-BTIN). A second AGR2 antibody (Cat#2533-1) was obtained from Epitomics and used for ELISA and western blot.

Cell treatments

DU145, MiaPaca-2, MCF7 and PC3 cells were synced by incubation for 16 h in serum free media prior to treatment. The incubation with drugs/compounds were performed for 30 min or 2 h with the following concentrations: 1 mM DTT, 5 µM tunicamycin, 100 nmol/l rAGR2, 100 nmole/l BSA, rapamycin 20 nmol/l, IGF1 40 ng/ml, EGF 20 ng/ml, and insulin 250 nmol/l.

Nuclear and cytoplasmic fractionation

Nuclear and cytoplasmic fractionations from DU145 cells (2×10^6) and MiaPaCa-2 cells (5×10^6) were obtained using NE-PER Nuclear and Cytoplasmic Reagents from Thermo Fisher Scientific.

AGR2 protein detection in spent media

Cells were grown for 48 h in media containing 1% FBS. The media was removed and filter sterilized with 0.45 µm syringe filter to remove debris. Levels of eAGR2 were assessed by TCA protein precipitation and immunoblot or by in ELISA [27].

AGR2 CRISPR-Cas9 knockout

PC3 ΔAGR2 and MCF7Δ AGR2 cell lines were made with CRISPR CAS9 and sgRNAs as previously described [27]. MCF7 was a heterozygous knockout and retained low levels of AGR2 while no AGR2 protein could be detected in heterozygous PC3 ΔAGR2 cells.

Spheroid formation assay

A total of 10,000 MiaPaCa-2 (GFP, ΔKTEL or AGR2) cells were plated into a CellCarrier™-96 Spheroid ULA/CS plate (PerkinElmer). Plates were centrifuged for 5 min at 3000 rpm. Cells were treated at time point zero (time of seeding) with 1 µmol/l OSI and or 100 ng/ml rAGR2 or PBS as control. Spheroids were observed after 24–96 h.

Co-immunprecipitation

Co-IPs were performed as previously described [28]. For the HA-RICTOR and AGR2 interaction, HEK293 cells were transfected with plasmids containing RICTOR mutants [41] or GFP as control using Lipofectamin 2000. Totally, 500 µg of lysate was incubated with 200 nM biotinylated rAGR2 and subject to Co-IP with 50 µl Pierce™ Streptavidin Magnetic Beads.

In vivo model

All animal procedures were performed according to an animal use and care protocol approved by the Institutional Care and Use Committee at the University of Southern California (A-3518-01). Mice were induced and maintained under 2% isoflurane in medical oxygen throughout all survival and imaging procedures.

Metastatic model of cancer

A total of 50,000 MiaPaCa-2 luciferase or CWR-22 Luciferase cells were re-suspended in 50 µl of sterile PBS. Under ultrasound guidance (Vevo2100, VisualSonics), cells were injected into the left ventricle of male athymic nude mice (Harlan Biosciences). Mice were maintained under 2% isoflurane in medical oxygen throughout the duration of the procedure. Firefly luciferin (50 mg/kg body weight) was administrated intravenously through the tail vein and tumor formation was determined by BLI using the IVIS 200 (PerkinElmer). Bioluminescence was analyzed using the Living Image Software 4.2 (PerkinElmer) and radiance quantified as photons/s/cm^2/sr. No animals were excluded. Greater than 80% power with $n = 10$ at per group, was used to test a large effect size of 3.1 at a two-sided type I error rate of 5%.

Subcutaneous xenograft model

Tumors were established in 8 male athymic nude mice per group (Harlan, Indianapolis) at 6 weeks old by injecting 1×10^6 DU145 (WT, C81S, ΔKTEL) cells in 100 µl of matrigel subcutaneously. Tumor growth was measured by using calipers to measure dimensions orthogonally. Volumes were calculated by the general equation of (SxL)/2, where S and L represent the small and large dimensions of the tumor lesions. No animals were excluded.

In vivo CT imaging

High resolution, small animal in vivo computed tomography (microCT) imaging was used to determine the intactness of bone structure (Simens Inveon MicroCT, Knoxville, TN). CT scans of the tibia region were acquired using the following settings: 80 kVp, 500 µA, 200 ms/180 steps covering 360°. Images were reconstructed into $768 \times 768 \times 512$ images, with an isotropic resolution of 0.105 mm.

AGR2 expression in CTC

Detailed methods for AGR2 expression in CTC-enriched peripheral blood using the CellSearch method is described [52, 53] with IRB approval/informed consent. CTCs were extracted from 7.5 ml of blood. Docetaxel response is defined as a ≥30% reduction in PSA at 12 weeks as suggested by PSAWG2 guidelines.

Statistical analysis

All experiments were performed at least three independent times unless otherwise indicated; sample size (n) is indicated in the legends. Data are expressed as average ± SD unless otherwise indicated. For in vivo experiments with $n = 3$ per group, we target 80% power to test a large effect size of 3.1 at a two-sided type I error rate of 5%. Results normally distributed with equal variance between groups were analyzed by unpaired two-tailed Student's t test. If variance was not similar between groups, Student's t test with unequal variances was applied. Asterisks or triangles denote p value significance. Sample sizes, statistical tests, and p values are indicated in the figure legends. All statistical analyses were calculated using JMP 12. The investigators were not blinded to the animal studies. For microscope images (spheroids) and immunoblots representative images of three independent experiments are shown.

Pathway analysis of interactome proteins

The Ingenuity Pathway Analysis (Qiagen, Inc.) import tool was used to incorporate IPI accession with a cutoff of $p < 0.05$. Unsupervised clustering of pathway analysis and corresponding—log p value was performed in R on using Euclidean distance and average-linkage (JMP Pro).

Data availability

Raw proteomics files have been deposited (https://goo.gl/N5NNuZ). Annotated supplemental tables include the final data and will be made available through BIOGRID.

Acknowledgments Drs. Philip Roux and Dos Sarbossov provided valuable insight and reagents (Roux) on the mTOR pathway. We are grateful for the guidance of Dr. David Agus and the generous financial support of the Lawrence J. Ellison Medical Foundation. We appreciate the support of Autumn Beemer, Lisa Flashner, Laura Ng, and Jeffrey Wang.

Compliance with ethical standards

Conflict of interest The authors declare that they have no conflict of interest.

References

1. Liu D, Rudland PS, Sibson DR, Platt-Higgins A, Barraclough R. Human homologue of cement gland protein, a novel metastasis inducer associated with breast carcinomas. Cancer Res. 2005;65:3796–805.
2. Patel P, Clarke C, Barraclough DL, Jowitt TA, Rudland PS, Barraclough R, et al. Metastasis-promoting anterior gradient 2 protein has a dimeric thioredoxin fold structure and a role in cell adhesion. J Mol Biol. 2012;425:929–43.
3. Park SW, Zhen G, Verhaeghe C, Nakagami Y, Nguyenvu LT, Barczak AJ, et al. The protein disulfide isomerase AGR2 is essential for production of intestinal mucus. Proc Natl Acad Sci USA. 2009;106:6950–5.
4. Higa A, Mulot A, Delom F, Bouchecareilh M, Nguyen DT, Boismenu D, et al. Role of pro-oncogenic protein disulfide isomerase (PDI) family member anterior gradient 2 (AGR2) in the control of endoplasmic reticulum homeostasis. J Biol Chem. 2011;286:44855–68.
5. Clarke C, Rudland P, Barraclough R. The metastasis-inducing protein AGR2 is O-glycosylated upon secretion from mammary epithelial cells. Mol Cell Biochem. 2015;408:245–52.
6. Fessart D, Domblides C, Avril T, Eriksson LA, Begueret H, Pineau R. et al. Secretion of protein disulphide isomerase AGR2 confers tumorigenic properties. Elife. 2016;5:1–24.
7. Wang Z, Hao Y, Lowe AW. The adenocarcinoma-associated antigen, AGR2, promotes tumor growth, cell migration, and cellular transformation. Cancer Res. 2008;68:492–7.
8. Fletcher GC, Patel S, Tyson K, Adam PJ, Schenker M, Loader JA, et al. hAG-2 and hAG-3, human homologues of genes involved in differentiation, are associated with oestrogen receptor-positive breast tumours and interact with metastasis gene C4.4a and dystroglycan. Br J Cancer. 2003;88:579–85.
9. Fritzsche FR, Dahl E, Dankof A, Burkhardt M, Pahl S, Petersen I, et al. Expression of AGR2 in non small cell lung cancer. Histol Histopathol. 2007;22:703–8.
10. Park K, Chung YJ, So H, Kim K, Park J, Oh M, et al. AGR2, a mucinous ovarian cancer marker, promotes cell proliferation and migration. Exp Mol Med. 2011;43:91–100.
11. Zhang JS, Gong A, Cheville JC, Smith DI, Young CY. AGR2, an androgen-inducible secretory protein overexpressed in prostate cancer. Genes Chromosomes Cancer. 2005;43:249–59.
12. Xu C, Liu Y, Xiao L, Guo C, Deng S, Zheng S, et al. The involvement of anterior gradient 2 in the stromal cell-derived factor 1-induced epithelial–mesenchymal transition of glioblastoma. Tumour Biol. 2016;37:6091–7.
13. Salmans ML, Zhao F, Andersen B. The estrogen-regulated anterior gradient 2 (AGR2) protein in breast cancer: a potential drug target and biomarker. Breast Cancer Res. 2013;15:204.
14. Mohtar MA, Hernychova L, O'Neill JR, Lawrence ML, Murray E, Vojtesek B, et al. The sequence-specific peptide-binding activity of the protein sulfide isomerase AGR2 directs its stable binding to the oncogenic receptor EpCAM. Mol Cell Proteom. 2018;17:737–63.
15. Brychtova V, Mohtar A, Vojtesek B, Hupp TR. Mechanisms of anterior gradient-2 regulation and function in cancer. Semin Cancer Biol. 2015;33:16–24.
16. Lee S, Bang S, Song K, Lee I. Differential expression in normal-adenoma-carcinoma sequence suggests complex molecular carcinogenesis in colon. Oncol Rep. 2006;16:747–54.
17. Zweitzig DR, Smirnov DA, Connelly MC, Terstappen LW, O'Hara SM, Moran E. Physiological stress induces the metastasis marker AGR2 in breast cancer cells. Mol Cell Biochem. 2007;306:255–60.
18. Chen R, Pan S, Duan X, Nelson BH, Sahota RA, de Rham S, et al. Elevated level of anterior gradient-2 in pancreatic juice from patients with pre-malignant pancreatic neoplasia. Mol Cancer. 2010;9:149.
19. Riener MO, Pilarsky C, Gerhardt J, Grutzmann R, Fritzsche FR, Bahra M, et al. Prognostic significance of AGR2 in pancreatic ductal adenocarcinoma. Histol Histopathol. 2009;24:1121–8.
20. Darb-Esfahani S, Fritzsche F, Kristiansen G, Weichert W, Sehouli J, Braicu I, et al. Anterior gradient protein 2 (AGR2) is an independent prognostic factor in ovarian high-grade serous carcinoma. Virchows Arch. 2012;461:109–16.
21. Rice GE, Edgell TA, Autelitano DJ. Evaluation of midkine and anterior gradient 2 in a multimarker panel for the detection of ovarian cancer. J Exp Clin Cancer Res. 2010;29:62.
22. Fritzsche FR, Dahl E, Pahl S, Burkhardt M, Luo J, Mayordomo E, et al. Prognostic relevance of AGR2 expression in breast cancer. Clin Cancer Res. 2006;12:1728–34.
23. Guo H, Zhu Q, Yu X, Merugu SB, Mangukiya HB, Smith N, et al. Tumor-secreted anterior gradient-2 binds to VEGF and FGF2 and enhances their activities by promoting their homodimerization. Oncogene. 2017;36:5098–109.
24. Arumugam T, Deng D, Bover L, Wang H, Logsdon CD, Ramachandran V. New blocking antibodies against novel AGR2-C4.4A pathway reduce growth and metastasis of pancreatic tumors and increase survival in mice. Mol Cancer Ther. 2015;14:941–51.
25. Tian S, Hu J, Tao K, Wang J, Chu Y, Li J, et al. Secreted AGR2 promotes invasion of colorectal cancer cells via Wnt11-mediated non-canonical Wnt signaling. Exp Cell Res. 2018;364:198–207.
26. Muniz VP, Barnes JM, Paliwal S, Zhang X, Tang X, Chen S, et al. The ARF tumor suppressor inhibits tumor cell colonization independent of p53 in a novel mouse model of pancreatic ductal adenocarcinoma metastasis. Mol Cancer Res. 2011;9:867–77.
27. Garri C, Howell S, Tiemann K, Tiffany A, Jalali-Yazdi F, Alba MM, et al. Identification, characterization and application of a new peptide against anterior gradient homolog 2 (AGR2). Oncotarget. 2018;9:27363–79.
28. Kani K, Garri C, Tiemann K, Malihi PD, Punj V, Nguyen AL, et al. JUN-Mediated downregulation of EGFR signaling is associated with resistance to gefitinib in EGFR-mutant NSCLC cell lines. Mol Cancer Ther. 2017;16:1645–57.
29. Kani K, Malihi PD, Jiang Y, Wang H, Wang Y, Ruderman DL, et al. Anterior gradient 2 (AGR2): Blood-based biomarker elevated in metastatic prostate cancer associated with the neuroendocrine phenotype. Prostate. 2013;73:306–15.

30. Roux KJ, Kim DI, Burke B. BioID: a screen for protein–protein interactions. Curr Protoc Protein Sci. 2013;74:Unit 19 23.
31. Tackett AJ, DeGrasse JA, Sekedat MD, Oeffinger M, Rout MP, Chait BT. I-DIRT, a general method for distinguishing between specific and nonspecific protein interactions. J Proteome Res. 2005;4:1752–6.
32. Mellacheruvu D, Wright Z, Couzens AL, Lambert JP, St-Denis NA, Li T, et al. The CRAPome: a contaminant repository for affinity purification-mass spectrometry data. Nat Methods. 2013;10:730–6.
33. Ryu J, Park SG, Lee PY, Cho S, Lee do H, Kim GH, et al. Dimerization of pro-oncogenic protein Anterior Gradient 2 is required for the interaction with BiP/GRP78. Biochem Biophys Res Commun. 2013;430:610–5.
34. Gray TA, Murray E, Nowicki MW, Remnant L, Scherl A, Muller P, et al. Development of a fluorescent monoclonal antibody-based assay to measure the allosteric effects of synthetic peptides on self-oligomerization of AGR2 protein. Protein Sci. 2013;22:1266–78.
35. Maslon MM, Hrstka R, Vojtesek B, Hupp TR. A divergent substrate-binding loop within the pro-oncogenic protein anterior gradient-2 forms a docking site for Reptin. J Mol Biol. 2010;404:418–38.
36. Matoulkova E, Sommerova L, Pastorek M, Vojtesek B, Hrstka R. Regulation of AGR2 expression via 3'UTR shortening. Exp Cell Res. 2017;356:40–7.
37. Fan R, Kim NG, Gumbiner BM. Regulation of Hippo pathway by mitogenic growth factors via phosphoinositide 3-kinase and phosphoinositide-dependent kinase-1. Proc Natl Acad Sci USA. 2013;110:2569–74.
38. Chan SW, Lim CJ, Guo K, Ng CP, Lee I, Hunziker W, et al. A role for TAZ in migration, invasion, and tumorigenesis of breast cancer cells. Cancer Res. 2008;68:2592–8.
39. Dong A, Gupta A, Pai RK, Tun M, Lowe AW. The human adenocarcinoma-associated gene, AGR2, induces expression of amphiregulin through Hippo pathway co-activator YAP1 activation. J Biol Chem. 2011;286:18301–10.
40. Laplante M, Sabatini DM. mTOR signaling in growth control and disease. Cell. 2012;149:274–93.
41. Julien LA, Carriere A, Moreau J, Roux PP. mTORC1-activated S6K1 phosphorylates Rictor on threonine 1135 and regulates mTORC2 signaling. Mol Cell Biol. 2010;30:908–21.
42. Boulbes D, Chen CH, Shaikenov T, Agarwal NK, Peterson TR, Addona TA, et al. Rictor phosphorylation on the Thr-1135 site does not require mammalian target of rapamycin complex 2. Mol Cancer Res. 2010;8:896–906.
43. Cancer Genome Atlas Network. Comprehensive molecular portraits of human breast tumours. Nature. 2012;490:61–70.
44. Cancer Genome Atlas Research Network. The molecular taxonomy of primary prostate cancer. Cell. 2015;163:1011–25.
45. Hengel SM, Murray E, Langdon S, Hayward L, O'Donoghue J, Panchaud A, et al. Data-independent proteomic screen identifies novel tamoxifen agonist that mediates drug resistance. J Proteome Res. 2011;10:4567–78.
46. Chung K, Nishiyama N, Yamano S, Komatsu H, Hanada S, Wei M, et al. Serum AGR2 as an early diagnostic and postoperative prognostic biomarker of human lung adenocarcinoma. Cancer Biomark. 2011;10:101–7.
47. Tohti M, Li J, Tang C, Wen G, Abdujilil A, Yizim P, et al. Serum AGR2 as a useful biomarker for pituitary adenomas. Clin Neurol Neurosurg. 2017;154:19–22.
48. Roux KJ, Kim DI, Raida M, Burke B. A promiscuous biotin ligase fusion protein identifies proximal and interacting proteins in mammalian cells. J Cell Biol. 2012;196:801–10.
49. Aceto N, Bardia A, Miyamoto DT, Donaldson MC, Wittner BS, Spencer JA, et al. Circulating tumor cell clusters are oligoclonal precursors of breast cancer metastasis. Cell. 2014;158:1110–22.
50. Lundberg E, Uhlen M. Creation of an antibody-based subcellular protein atlas. Proteomics. 2010;10:3984–96.
51. Jia M, Guo Y, Zhu D, Zhang N, Li L, Jiang J, et al. Pro-metastatic activity of AGR2 interrupts angiogenesis target bevacizumab efficiency via direct interaction with VEGFA and activation of NF-kappaB pathway. Biochim Biophys Acta. 2018;1864(5 Pt A):1622–33.
52. Jiang Y, Palma JF, Agus DB, Wang Y, Gross ME. Detection of androgen receptor mutations in circulating tumor cells in castration-resistant prostate cancer. Clin Chem. 2010;56:1492–5.
53. Smirnov DA, Zweitzig DR, Foulk BW, Miller MC, Doyle GV, Pienta KJ, et al. Global gene expression profiling of circulating tumor cells. Cancer Res. 2005;65:4993–7.
54. Skarra DV, Goudreault M, Choi H, Mullin M, Nesvizhskii AI, Gingras AC, et al. Label-free quantitative proteomics and SAINT analysis enable interactome mapping for the human Ser/Thr protein phosphatase 5. Proteomics. 2011;11:1508–16.
55. Scher HI, Halabi S, Tannock I, Morris M, Sternberg CN, Carducci MA, et al. Design and end points of clinical trials for patients with progressive prostate cancer and castrate levels of testosterone: recommendations of the Prostate Cancer Clinical Trials Working Group. J Clin Oncol. 2008;26:1148–59.